Electron tunneling in biological molecules*

Jay R. Winkler, Angel J. Di Bilio, Neil A. Farrow, John H. Richards and Harry B. Gray[†]

Beckman Institute, California Institute of Technology, Pasadena, CA 91125, USA

Abstract: Electron transfers in photosynthesis and respiration commonly occur between protein-bound prosthetic groups that are separated by large molecular distances (often greater than 10 Å). Although the electron donors and acceptors are expected to be weakly coupled, the reactions are remarkably fast and proceed with high specificity. Tunneling timetables based on analyses of Fe^{2+}/Cu^+ to Ru^{3+} electron-transfer rates for Ru-modified heme and copper proteins reveal that the structure of the intervening polypeptide can control these distant donor–acceptor couplings. Multistep tunneling can account for the relatively rapid Cu^+ to Re^{2+} electron transfer observed in Re-modified azurin.

INTRODUCTION

Electron tunneling occurs in reactions where the electronic interaction between redox sites is relatively weak [1]. Under these circumstances, the transition state for the electron-transfer reaction must be formed many times before there is a successful conversion from reactants to products. Semiclassical theory (Eqn 1) [2] predicts that the reaction

$$k_{ET} = (4\pi^3/h^2\lambda k_B T)^{1/2} H_{AB}^2 \exp[-(\Delta G^0 + \lambda)^2/4\lambda k_B T] \qquad (1)$$

rate for electron transfer (ET) from a donor (D) to an acceptor (A) at fixed separation and orientation depends on the reaction driving force ($-\Delta G°$), a nuclear reorganization parameter (λ), and the electronic-coupling strength between reactants and products at the transition state (H_{AB}). This theory reduces a complex dynamical problem in multidimensional nuclear-configuration space to a simple expression comprised of just two parameters (λ, H_{AB}). Equation 1 naturally partitions into nuclear (exponential) and electronic (pre-exponential) terms: ET rates reach their maximum values (k_{ET}^o) when the nuclear factor is optimized ($-\Delta G° = \lambda$); these k_{ET}^o values are limited only by the electronic-coupling strength (H_{AB}^2).

Ru-MODIFIED PROTEINS

Investigations of the driving-force, temperature, and distance dependences of ET rates can be used to define the fundamental ET parameters λ and H_{AB} [3–10]. Natural systems often are not amenable to the systematic studies that are required to explore the fundamental aspects of biological ET reactions [11]. Indeed, some of the most revealing investigations have employed chemically modified proteins [1,11–34]. One particularly successful approach has involved measurements of ET in metalloproteins that have been surface-labeled with $Ru(bpy)_2(im)(HisX)^{2+}$ (bpy = 2,2'-bipyridine; im = imidazole) (Fig. 1) [19–27]. The long-lived, luminescent Ru-to-bpy charge-transfer excited states enable a wider range of electron-transfer measurements than is possible with nonluminescent complexes [19,24]. Furthermore, the bpy ligands raise the $Ru^{3+/2+}$ reduction potential to ≈ 1 V vs. NHE, so that $Fe^{2+} \rightarrow Ru^{3+}$ and $Cu^+ \rightarrow Ru^{3+}$ ET rates are closer to k_{ET}^o, leading to more reliable estimates of H_{AB} and λ [1].

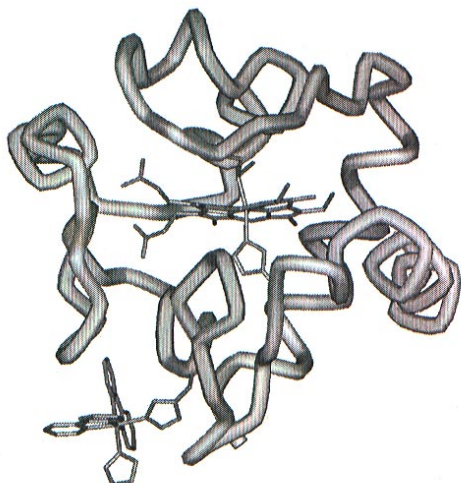† *Correspondence:* E-mail: hgcm@its.caltech.edu

Fig. 1 Model of Ru(bpy)$_2$(im)(His33)-cytochrome *c*.

REORGANIZATION ENERGY

The nuclear factor in Eqn 1 results from a classical treatment of nuclear motions in which all reorganization is described by a single harmonic coordinate. The parameter λ is defined as the energy of the reactants at the equilibrium nuclear configuration of the products. The remarkable aspect of the nuclear factor is the predicted free-energy dependence (Fig. 2). At low driving forces, rates increase with $-\Delta G°$ but, at very high driving forces ($-\Delta G° > \lambda$), ET rates are predicted to decrease (inverted effect). Experimental studies of electron-transfer rates in synthetic model complexes [3–5,7,9,10] and in biological systems [15,22,31,33] have provided convincing evidence for inverted driving-force effects.

$$k_{ET} = \sqrt{\frac{4\pi^3}{h^2 \lambda k_B T}}\; H_{AB}^2\; exp\left[-\frac{(\Delta G° + \lambda)^2}{4\lambda k_B T} \right]$$
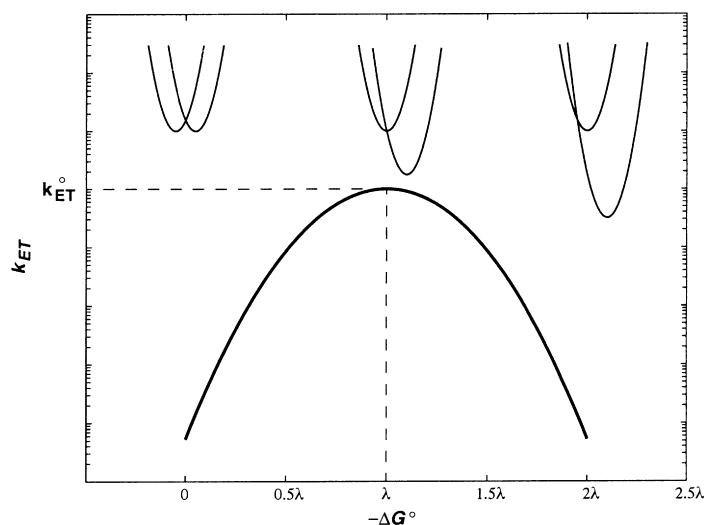

Fig. 2 Driving-force dependence of nonadiabatic electron-transfer rates predicted by semiclassical electron-transfer theory. Reactant-product potential-energy surfaces for the normal (left), driving force optimized (middle) and inverted (right) regions appear above the curve. The equation describes the rate as a function of driving force ($-\Delta G°$), reorganization energy (λ), and the reactant-product electronic coupling strength (H_{AB}).

For ET reactions in polar solvents, the dominant contribution to λ arises from reorientation of solvent molecules in response to the change in charge distribution of the reactants (λ_S). Dielectric continuum models are commonly used in calculations of solvent reorganization. The earliest models treated the reactants as conducting spheres [2]; later refinements dealt with charge shifts inside low dielectric cavities of regular (spherical, ellipsoidal) shape [35,36]. Embedding reactants in a low dielectric medium (e.g. a membrane) can dramatically reduce reorganization energies, but the effect on ET rates depends on the response of $-\Delta G°$ to the nonpolar environment. Generally, low dielectric media will reduce the driving force for charge-separation reactions ($D + A \rightarrow D^+ + A^-$), but will have a smaller effect on the energetics of charge-shift reactions (e.g. $D^- + A \rightarrow D + A^-$).

The second component of the nuclear factor arises from changes in bond lengths and bond angles of the donor and acceptor following electron transfer. Classical descriptions of this inner-sphere reorganization (λ_I) usually are not adequate, and quantum-mechanical refinements to Eqn 1 have been developed [37]. The most significant consequences of quantized nuclear motions are found in the inverted region. Owing to nuclear tunneling through the activation barrier, highly exergonic reactions will not be as slow as predicted by the classical model. Distortions along coordinates associated with high-frequency vibrations ($> 1000\ \mathrm{cm}^{-1}$) can significantly attenuate the inverted effect.

The nuclear factor reflects the interplay between driving force and reorganization energy that regulates ET rates. A reaction in the inverted region can be accelerated if a pathway is available that releases less free energy in the actual ET step. This can be accomplished by the formation of electronically excited products ($^*D^+$, $^*A^-$), because the ET driving force will be lower by an amount equal to the energy of the excited electronic state. An ET process that forms excited products will be the preferred pathway if its driving force is closer to λ than that of a reaction forming ground-state products [38].

The driving-force dependence of intramolecular ET rates in Ru(NH$_3$)$_4$L(His33)-Zn-cyt c (L = NH$_3$, pyridine, isonicotinamide) indicates $\lambda = 1.15$ eV and $H_{AB} = 0.1\ \mathrm{cm}^{-1}$ [39]. Studies of self-exchange reactions have demonstrated that replacing ammonia ligands with diimine ligands substantially reduces the reorganization energy associated with Ru$^{3+/2+}$ ET [40]. The difference can be attributed to a decrease in solvent polarization by the larger Ru-diimine ions, and to somewhat smaller inner-sphere barriers as well. It was expected, then, that the reorganization energy for ET in Ru(bpy)$_2$(im)(His33)-Fe-cyt c (bpy = 2,2'-bipyridine) would be less than 1.2 eV; a cross-relation calculation suggested a value of 0.8 eV. Analysis of the driving-force dependence of Fe$^{2+}\rightarrow$Ru^{3+} ET rates in Ru(LL)$_2$(im)(His33)-Fe-cyt c (LL = bpy, 4,4'-(CH$_3$)$_2$-bpy, 4,4',5,5'-(CH$_3$)$_4$-bpy, 4,4'-(CONH(C$_2$H$_5$))$_2$-bpy) gives $\lambda = 0.76$ eV, which is in excellent agreement with this estimate (Fig. 3) [22].
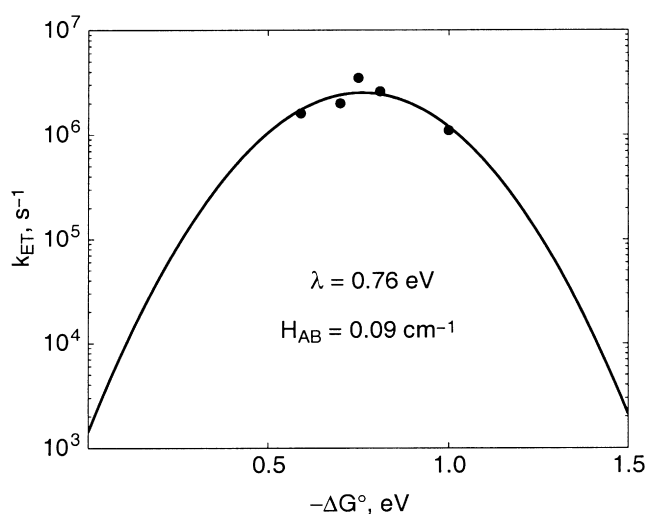
Fig. 3 Driving-force dependence of electron-transfer rates in Ru(bpy)$_2$(im)(His33)-cytochrome c [22]. Solid curve was calculated using Eqn 1 with the indicated parameters.

The significant difference in reorganization energy between Ru-ammine and Ru-bpy modified proteins highlights the important role of water in protein electron transfer. The bulky bpy ligands shield the charged metal center from the polar aqueous solution, reducing the solvent reorganization energy. In the same manner, the medium surrounding a metalloprotein active site will affect the reorganization energy associated with its ET reactions. A hydrophilic active site will lead to larger reorganization energies than a hydrophobic site. Consequently, the kinetics of protein ET reactions will be very sensitive to the active-site environment.

ELECTRONIC COUPLING

Nonadiabatic ET reactions are characterized by weak electronic interaction between the reactants and products at the transition-state nuclear configuration ($H_{AB} << k_B T$). This coupling is directly related to the strength of the electronic interaction between the donor and acceptor [41]. When donors and acceptors are separated by long distances ($> 10 \text{ Å}$), the D/A interaction will be quite small.

In 1974 Hopfield described biological ET in terms of electron tunneling through a square potential barrier [42]. In this model, H_{AB}^2 (and, hence, k_{ET}) drops off exponentially with increasing D-A separation. The height of the tunneling barrier relative to the energies of the D/A states determines the distance-decay constant (β). A decay constant in the range of $3.5–5 \text{ Å}^{-1}$ has been estimated for donors and acceptors separated by a vacuum and, as a practical matter, ET is prohibitively slow at D-A separations (R) greater than 8 Å ($k_{ET}^o < 10 \text{ s}^{-1}$). An intervening medium between redox sites reduces the height of the tunneling barrier, leading to a smaller distance-decay constant. Hopfield estimated $\beta \approx 1.4 \text{ Å}^{-1}$ for biological ET reactions on the basis of measurements of the temperature dependence of ET from a cytochrome to the oxidized special pair in the photosynthetic reaction center of *Chromatium vinosum* [42]. An 8 Å edge-edge separation was estimated on the basis of this decay constant; later structural studies revealed that the actual distance was somewhat greater (12.3 Å).

The square-barrier models assume that the distant couplings result from direct overlap of localized donor and acceptor wavefunctions. In long-range ET ($R > 10 \text{ Å}$), the direct interaction between donors and acceptors is negligible; electronic states of the intervening bridge mediate the coupling *via* superexchange. If oxidized states of the bridge mediate the coupling, the process is referred to as 'hole transfer'; mediation by reduced bridge states is known as 'electron transfer'. In 1961 McConnell developed a superexchange coupling model to describe charge–transfer interactions between donors and acceptors separated by spacers comprised of m identical repeat units (Eqn 2) [43]. The total coupling depends upon the interaction between adjacent hole

$$H_{AB} = (h_D/\Delta)(h_j/\Delta)^{m-1} h_A \tag{2}$$

or electron states in the bridge (h_j), the energy difference between the degenerate D/A states and the bridge states (Δ), and the interactions between the D and A states and the bridge (h_D, h_A). This model assumes that only nearest-neighbor interactions mediate the coupling and, consequently, predicts that H_{AB} will vary exponentially with the number of repeat units in the bridge. Several studies of the distance dependence of ET in synthetic donor-acceptor complexes agree quite well with this prediction [44–46]. *Ab initio* calculations of H_{AB} for bridges composed of saturated alkane spacers, however, suggest that the simple superexchange model is not quantitatively accurate [47–50]. Nonnearest-neighbor interactions were found to dominate the couplings and, except in a few cases, nearest–neighbor interactions were relatively unimportant. A particularly significant finding in these studies is that the non-nearest neighbor interactions make the coupling along a saturated alkane bridge quite sensitive to its conformation.

The medium separating redox sites in proteins is comprised of a complex array of bonded and nonbonded contacts and an *ab initio* calculation of coupling strengths is a formidable challenge. The homologous-bridge superexchange model (Eqn 2) is not suitable because of the diverse interactions in proteins. Beratan, Onuchic, and co-workers developed a generalization of the McConnell superexchange coupling model that accommodates the structural complexity of a protein matrix [51–55]. In this tunneling-pathway model, the medium between D and A is decomposed into smaller subunits linked by covalent bonds, hydrogen bonds, or through-space jumps. Each link is assigned a coupling decay (ϵ_C, ϵ_H,

ϵ_S), and a structure-dependent searching algorithm is used to identify the optimum coupling pathway between the two redox sites. The total coupling of a single pathway is given as a repeated product of the couplings for the individual links (Eqn 3).

$$H_{AB} \propto \Pi\epsilon_C\Pi\epsilon_H\Pi\epsilon_S \tag{3}$$

A tunneling pathway can be described in terms of an effective covalent tunneling path comprised of n (nonintegral) covalent bonds, with a total length equal to σ_l (Eqn 4). The relationship between σ_l and the direct D-A distance(R) reflects

$$H_{AB} \propto (\epsilon_C)^n \tag{4a}$$

$$\sigma_l = n \times 1.4 \text{ Å/bond} \tag{4b}$$

the coupling efficiency of a pathway [23]. The variation of ET rates with R depends upon the coupling decay for a single covalent bond (ϵ_C), and the magnitude of ϵ_C depends critically upon the energy of the tunneling electron relative to the energies of the bridge hole and electron states [56]. In considering ET data from different protein systems, then, care must be taken to compare reactions in which oxidants (for hole tunneling) have similar reduction potentials.

The tunneling-pathway model has proven to be one of the most useful methods for estimating long-range electronic couplings [51–53,57,58]. Employing this model, Beratan, Betts, and Onuchic predicted in 1991 that proteins comprised largely of β-sheet structures would be more effective at mediating long-range couplings than those built from α helices [55]. This analysis can be taken a step further by comparing the coupling efficiencies of individual protein secondary structural elements (β strands, α helices). The coupling efficiency can be determined from the variation of σ_l as a function of R. A linear σ_l/R relationship implies that k_{ET}^o will be an exponential function of R; the distance-decay constant is determined by the slope of the σ_l/R plot and the value of ϵ_C.

A β sheet is comprised of extended polypeptide chains interconnected by hydrogen bonds; the individual strands of β sheets define nearly linear coupling pathways along the peptide backbone spanning 3.4 Å per residue. The tunneling length for a β strand exhibits an excellent linear correlation with β-carbon separation (R_β); the best linear fit with zero intercept yields a slope of 1.37 σ_l/R_β (distance-decay constant = 1.0 Å^{-1}; Fig. 4). Couplings across a β sheet depend upon the ability of hydrogen bonds to mediate the D/A interaction. The standard parameterization of the tunneling-pathway model defines the coupling decay across a hydrogen bond in terms of the heteroatom separation (Eqn 4). If the two heteroatoms are separated by twice the 1.4-Å covalent-bond distance,

$$\epsilon_H = \epsilon_C^2 \exp[-1.7(R - 2.8)] \tag{5}$$

then the hydrogen-bond decay is assigned a value equal to that of a covalent bond [53]. Longer heteroatom separations lead to weaker predicted couplings but, as yet, there is no experimental confirmation of this relationship.

In the coiled α-helix structure a linear distance of just 1.5 Å is spanned per residue. In the absence of mediation by hydrogen bonds, σ_l is a very steep function of R_β, implying that an α helix is a poor conductor of electronic coupling (2.7 σ_l/R_β, distance-decay constant = 1.97 Å^{-1}) [23]. If the hydrogen-bond networks in α helices mediate coupling, then the Beratan–Onuchic parameterization of hydrogen-bond couplings suggests a σ_l/R_β ratio of 1.72 (distance-decay constant = 1.26 Å^{-1}; Fig. 4). Treating hydrogen bonds as covalent bonds further reduces this ratio (1.29 σ_l/R_β, distance-decay constant = 0.94 Å^{-1}). Hydrogen–bond interactions, then, will determine whether α helices are vastly inferior to or are slightly better than β sheets in mediating long-range electronic couplings. It is important to note that the coiled helical structure leads to poorer σ_l/R_β correlations, especially for values of R_β under 10 Å. In this distance region, the tunneling pathway model predicts little variation in coupling efficiencies for the different secondary structures. The coupling in helical structures could be highly anisotropic. Electron transfer along a helix may have a very different distance dependence from ET across helices. In the latter cases, the coupling efficiency will depend on the nature of the interactions between helices. A final point involves the dependence of coupling efficiencies on bond angles. It is well known that β sheets and α
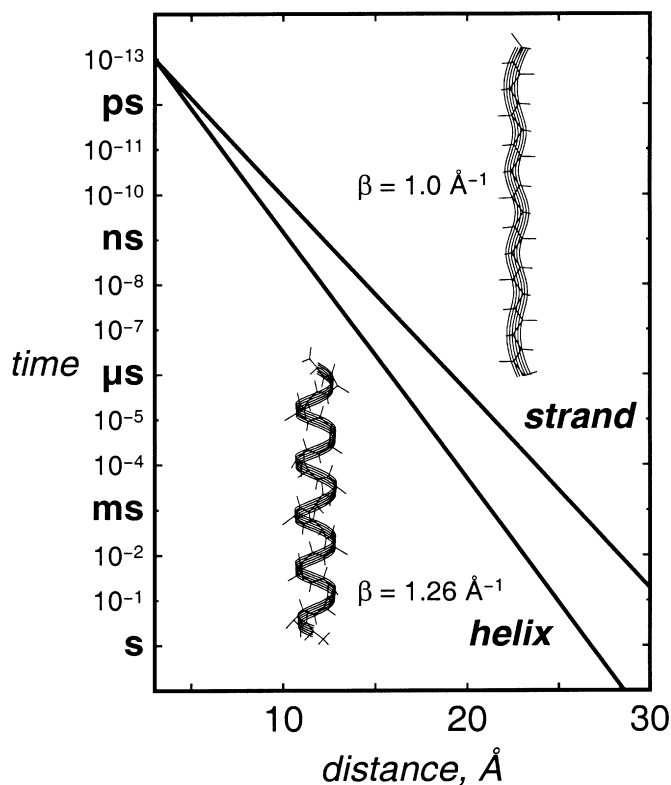
Fig. 4 Tunneling pathway predictions of the distance dependence of tunneling times for electron transfer along a β strand and an α helix.

helices are described by quite different peptide bond angles (ϕ, ψ). *Ab initio* calculations on saturated hydrocarbons have suggested that different conformations provide different couplings [47]. Different values of ϵ_C, then, might be necessary to describe couplings in β sheets and α helices.

TUNNELING TIMETABLES

Analyses of ET rate/distance relationships require a consistent definition of the D-A distance [59–61]. When comparing rates from systems with different donors and/or acceptors, it can be difficult to identify a proper distance measure. All maximum ET rates should extrapolate to a common adiabatic rate as R approaches van der Waals contact. So-called edge-to-edge distances are often employed but there are many ambiguities, not the least of which is defining the sets of atoms that constitute the edges of D and A. For planar aromatic molecules (e.g. chlorophylls, pheophytins, quinones), edge-edge separations are usually defined on the basis of the shortest distance between aromatic carbon atoms of D and A. In transition-metal complexes (e.g. Fe-heme, Ru-ammine, Ru-bpy), however, atoms on the periphery are not always well coupled to the central metal, and empirical evidence suggests that metal-metal distances are more appropriate.

Coupling-limited rates (k_{ET}^o) have been obtained for Ru-modified azurin mutants with His residues at different sites on the β strands extending from Met121 (His122, His124, His126) and Cys112 (His109, His107) [23,56,62–64]. The variation of tunneling time with the Cu-Ru separation (exponential decay constant of $1.1\,\text{Å}^{-1}$) is in remarkably good agreement with the predicted value of $1.0\,\text{Å}^{-1}$ for a strand of an ideal β sheet (Fig. 5). Detailed electronic structure calculations indicate that the S atom of Cys112 has by far the strongest coupling to the Cu center; the His (imidazole) couplings are only one third that of the Cys ligand, and the Met121 (S) and Gly45 (O) couplings are just a tenth of the Cys coupling [65,66]. These highly anisotropic ligand interactions strongly favor pathways that couple to the Cu through Cys112. Couplings along different β strands would be
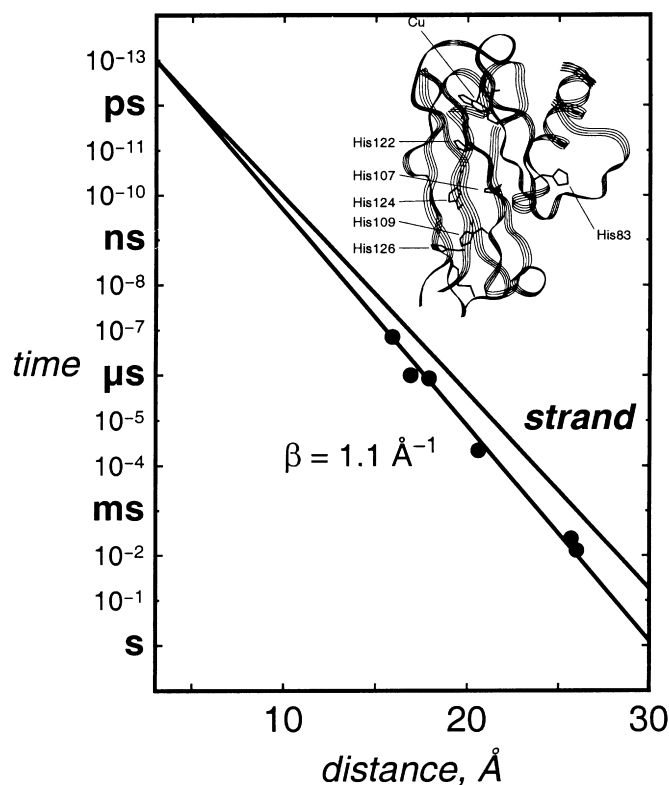
Fig. 5 Tunneling timetable for six different Ru-modified azurins. One solid line shows the best linear fit with an intercept at 13 and corresponds to a distance decay parameter of 1.1 Å^{-1}; the other line shows the tunneling-pathway prediction for coupling along a β strand.

expected to have the same distance-decay constants, but different intercepts at close contact. In this light, then, it is quite surprising that the distance dependence of ET in Ru-modified azurin can be described by a single straight line (Fig. 5).

One explanation for uniform distance dependence of couplings along the Met121 and Cys112 strands is that strong interstrand hydrogen bonds serve to direct all of the distant couplings through the Cys112 ligand [56,67,68]. A hydrogen bond between Met121(O) and Cys112(NH) could mediate coupling from the Ru complex bound to His122. A second hydrogen bond (Gly123(O)-Phe110(NH)) would provide a coupling link for His124 and His126 ET reactions. The importance of the pathways that cross from the Met121 strand to the Cys112 strand depends upon the coupling efficiencies of the hydrogen bonds. Model-complex studies have demonstrated efficient electron transfer across hydrogen-bonded interfaces [69,70]. In the standard Beratan-Onuchic pathway model, hydrogen-bond couplings are distance-scaled and generally afford weaker couplings than covalent bonds [53]. This procedure for calculating hydrogen-bond couplings cannot explain the similar distance dependences of ET along the Met121 and Cys112 strands in Ru-modified azurins. Treating the hydrogen bonds as covalent bonds in the tunneling-pathway model ($\epsilon_H = \epsilon_C^2$), however, does lead to better agreement with experiment [56].

Long-range ET from the Cys3-Cys26 disulfide radical anion to the copper in azurin has been studied extensively by Farver and Pecht [71,72]. Estimates based on experimental rate data indicate that the S_2/Cu coupling is unusually strong for a donor/acceptor pair separated by 26 Å. Relatively strong Cu/Ru couplings also have been found for ET reactions involving Ru-modified His83 [56,62,63]. Interestingly, both the Cys3-Cys26 and His83 tunneling times fit on the 1.1 Å^{-1} distance decay defined by the couplings along the Met121 and Cys112 strands (Fig. 5). Strong interstrand hydrogen bonds may be responsible for the efficient couplings from the disulfide site and from His83 [63].

Donor-acceptor pairs separated by α helices include the heme-Ru redox sites in two Ru-modified myoglobins, Ru(bpy)$_2$(im)(HisX)-Mb (X = 83, 95; Fig. 6) [73,74]. The tunneling pathway from His95 to the Mb-heme is comprised of a short section of α helix terminating at His93, the heme axial ligand. The coupling for the [Fe^{2+} → Ru^{3+}(His95)]-Mb ET reaction [73] is of the same magnitude as that found in Ru-modified azurins with comparable D-A spacings. This result is consistent with the tunneling-pathway model, which predicts very little difference in the coupling efficiencies of α helices and β sheets at small D-A separations. The [Fe^{2+} → Ru^{3+}(His83)]-Mb [74] tunneling time, however, is substantially longer than those found in β-sheet structures at similar separations, in accord with the predicted distance-decay constant for an α helix (Fig. 6).
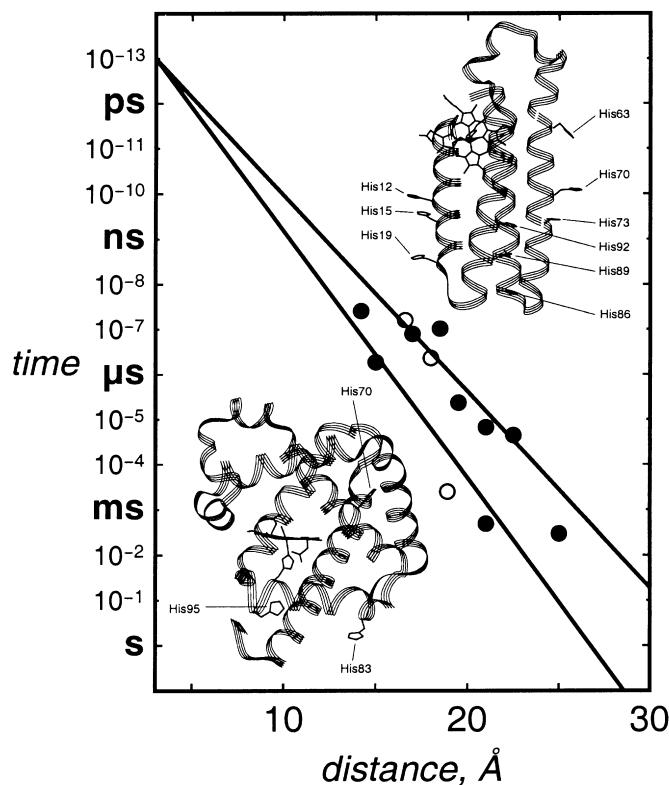

Fig. 6 Tunneling timetable for Ru-modified cytochrome b_{562} (filled circles) and myoglobin (open circles). Solid lines are the tunneling-pathway predictions for coupling along a β strand (upper) and α helix (lower).

ET rate data are available for nine Ru-modified derivatives of cytochrome b_{562}, a four-helix-bundle protein [75]. The tunneling times for Ru-modified b_{562} exhibit far more scatter than was found for Ru-modified azurin. Two derivatives exhibit ET rates close to those predicted for coupling along a simple α helix, and several others lie close to the β-strand decay. In these proteins, as in Ru(His70)Mb, the intervening medium is not a simple section of α helix. Coupling across helices, perhaps on multiple interfering pathways, is likely to produce a complex distance dependence. Interpretation of the relative ET rates in cytochrome b_{562} will require a more detailed analysis of the medium separating the redox sites [76].

The master tunneling timetable for Ru-modified proteins (Fig. 7) demonstrates that virtually all observed ET rates fall in a zone bound by the predicted distance decays for α helices and β strands. This large set of kinetics data provides compelling support for tunneling mediated by the sigma-bond framework of the protein. Measured protein ET rates that lie outside of this zone should be examined carefully for possible alternative mechanisms.
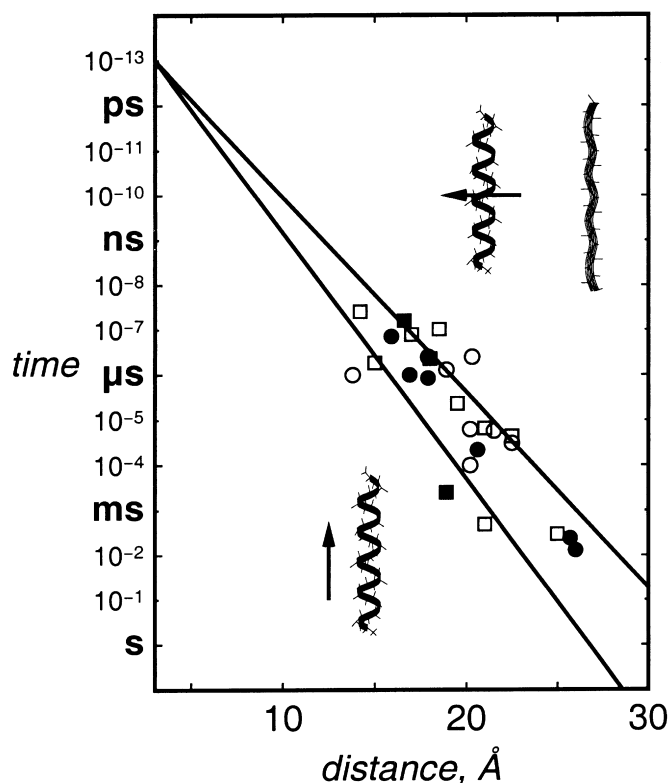
Fig. 7 Tunneling timetable for four proteins: Ru-modified azurin data (filled circles) [23,56,64]: [Ru-label site, k_{ET}° s^{-1}, R Å] His122, 7.1×10^6, 15.9; His124, 2.2×10^4, 20.6; His126, 1.3×10^2, 26.0; His109, 8.5×10^5, 17.9; His107, 2.4×10^2, 25.7; His83 1.0×10^6, 16.9. Ru-modified cyt *c* data (open circles) [23]: His39, 2.5×10^6, 20.3; His33, 2.5×10^6, 17.9; His66, 1.3×10^6, 18.9; His72, 1.0×10^6, 13.8; His58, 6.3×10^4, 20.2; His62, 1.0×10^4, 20.2; His54, 3.1×10^4, 22.5; His54(Ile52), 5.8×10^4, 21.5. Ru-modified myoglobin data (filled squares) [73,74]: His83 2.5×10^3, 18.9; His95 2.3×10^6, 18.0; His70 1.6×10^7, 16.6. Ru-modified cytochrome b_{562} data (open squares) [75]: His12, 2.6×10^7, 14.2; His15, 1.9×10^6, 15.0; His19, 6.7×10^4, 21.0; His63, 7.9×10^6, 17.0; His70, 2.3×10^5, 19.5; His73, 4.9×10^2, 21.0; His86, 2.9×10^2, 25.0; His89, 4.4×10^4, 22.5; His92, 1.0×10^7, 18.5.

MULTISTEP TUNNELING

Electron tunneling in proteins is relatively slow at very long molecular distances (Fig. 7). Experimentally validated tunneling times for distances greater than 25 Å are milliseconds or greater, as exemplified by Ru(His107)-azurin. In this protein, calculations show that a multistep tunneling ('hopping') mechanism through an intervening Tyr108 ($Cu^+ \rightarrow Tyr^{+/0} \rightarrow Ru^{3+}$) is only slightly less favorable than direct $Cu^+ \rightarrow Ru^{3+}$ tunneling. In order to examine multistep tunneling experimentally, we have modified the His107 mutant of azurin with $Re(CO)_3(phen)(H_2O)^+$ (phen = 1,10-phenanthroline) [77]. With a high-potential oxidant at position 107 (the reduction potential of $Re(CO)_3(phen)(im)^{2+/+}$ is 2.1 V vs. (NHE) [78], rapid generation of Tyr108$^{\bullet +}$ is followed by rate-limiting $Cu^+ \rightarrow Tyr108^{\bullet +}$ tunneling (Fig. 8). Reasonable estimates for the Tyr108$^{\bullet +/0}$ reduction potential and λ-values give a $Cu^+ \rightarrow Tyr108^{\bullet +}$ tunneling rate (1.5×10^5 s^{-1}) that is three orders of magnitude greater than that for optimized $Cu^+ \rightarrow Re^{2+}$ tunneling.

We have exploited the flash/quench method to generate Re(His107)$^{2+}$-azurin(Cu$^+$), which rapidly forms Re(His107)$^+$-azurin(Cu^{2+}) (Fig. 9). The rate of Cu$^+$ oxidation (2×10^4 s^{-1}) is in reasonable agreement with that predicted for $Cu^+ \rightarrow Tyr108^{\bullet +}$ tunneling and, importantly, is much greater than the rate of direct $Cu^+ \rightarrow Ru^{3+}$ tunneling in Ru(His107)-azurin. Work in progress with Re(His107)-Zn-azurin is aimed at a direct measurement of the Tyr $\rightarrow$ Re^{2+} ET rate.
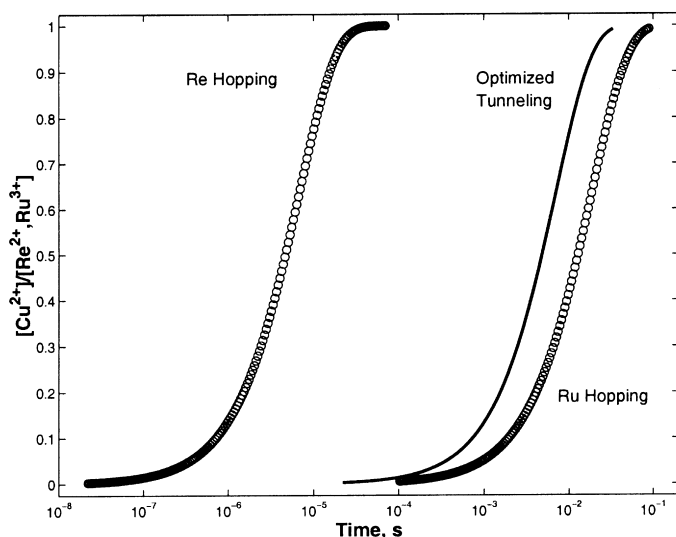
Fig. 8 Simulated kinetics of Cu^{2+} formation in M(His107)-azurin (M = Re and Ru) in the single-step (solid line) and multistep (circles) tunneling limits. The single-step tunneling reaction was assumed to be driving-force optimized ($-\Delta G° = \lambda = 0.8$ eV) with a distance decay factor $\beta = 1.1$ Å^{-1} and a metal–metal separation distance of 25.7 Å. Multistep tunneling was assumed to proceed via oxidation of Tyr108 (11.0 Å from M; 19.3 Å from Cu). The following parameters were employed in the multistep tunneling simulations: Tyr→M, $\lambda = 1.0$ eV and $\Delta G° = 0.2$ eV (M = Ru), $\Delta G° = –0.9$ eV (M = Re); Cu^+→Tyr$^•$ $\lambda = 1.0$ eV and $\Delta G° = –0.9$ eV. Approximate Cu^{2+} formation rate constants are 1.4×10^2 s^{-1} (optimized tunneling), 5.4×10^1 s^{-1} (Ru multistep tunneling), 1.5×10^5 s^{-1} (Re multistep tunneling).
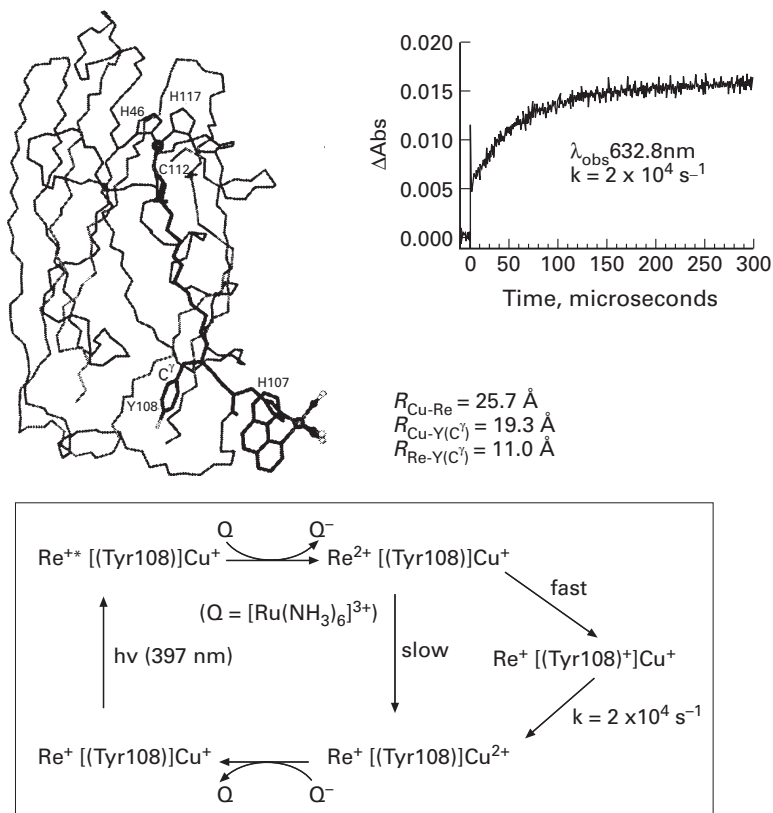

Fig. 9 Model of Ru(phen)(CO)$_3$(His107)-azurin (upper left); kinetics of $Cu^+ \rightarrow Re^{2+}$ ET (upper right); and proposed mechanism for multistep tunneling via Tyr108 (lower panel).

ACKNOWLEDGEMENTS

REFERENCES

1   H. B. Gray, J. R. Winkler. *Annu. Rev. Biochem.* **65**, 537–561 (1996).

2   R. A. Marcus, N. Sutin. *Biochim. Biophys. Acta* **811**, 265–322 (1985).

3   G. L. Closs, L. T. Calcaterra, N. J. Green, K. W. Penfield, J. R. Miller. *J. Phys. Chem.* **90**, 3673–3683 (1986).

4   G. L. Closs, J. R. Miller. *Science* **240**, 440–447 (1988).

5   L. S. Fox, M. Kozik, J. R. Winkler, H. B. Gray. *Science* **247**, 1069–1071 (1990).

6   P. Finckh, H. Heitele, M. Volk, M. E. Michel-Beyerle. *J. Phys. Chem.* **92**, 6584–6590 (1988).

7   D. Wiedenfeld, M. Bachrach, T. M. McCleskey, M. G. Hill, H. B. Gray, J. R. Winkler. *J. Phys. Chem. B* **101**, 8823–8826 (1997).

8   K. D. Jordan, M. N. Paddon-Row. *Chem. Rev.* **92**, 395–410 (1992).

9   M. R. Wasielewski, M. P. Niemczyk, W. A. Svec, E. B. Pewitt. *J. Am. Chem. Soc.* **107**, 1080–1082 (1985).

10   P. Chen, R. Duesing, D. K. Graff, T. J. Meyer. *J. Phys. Chem.* **95**, 5850–5858 (1991).

11   H. B. Gray, B. G. Malmström. *Biochemistry* **28**, 7499–7505 (1989).

12   J. R. Winkler, D. G. Nocera, K. M. Yocom, E. Bordignon, H. B. Gray. *J. Am. Chem. Soc.* **104**, 5798–5800 (1982).

13   S. S. Isied, C. Kuehn, G. Worosila. *J. Am. Chem. Soc.* **106**, 1722–1726 (1984).

14   J. L. McGourty, N. V. Blough, B. M. Hoffman. *J. Am. Chem. Soc.* **105**, 4470–4472 (1983).

15   G. McLendon, J. R. Miller. *J. Am. Chem. Soc.* **107**, 7811–7816 (1985).

16   M. R. Gunner, D. E. Robertson, P. L. Dutton. *J. Phys. Chem.* **90**, 3783–3795 (1986).

17   H. B. Gray. *Chem. Soc. Rev.* **15**, 17–30 (1986).

18   M. P. Jackman, J. McGinnis, R. Powls, G. A. Salmon, A. G. Sykes. *J. Am. Chem. Soc.* **110**, 5880–5887 (1988).

19   I.-J. Chang, H. B. Gray, J. R. Winkler. *J. Am. Chem. Soc.* **113**, 7056–7057 (1991).

20   D. S. Wuttke, M. J. Bjerrum, J. R. Winkler, H. B. Gray. *Science* **256**, 1007–1009 (1992).

21   D. R. Casimiro, J. H. Richards, J. R. Winkler, H. B. Gray. *J. Phys. Chem.* **97**, 13073–13077 (1993).

22   G. A. Mines, M. J. Bjerrum, M. G. Hill, D. R. Casimiro, I.-J. Chang, J. R. Winkler, H. B. Gray. *J. Am. Chem. Soc.* **118**, 1961–1965 (1996).

23   R. Langen, I.-J. Chang, J. P. Germanas, J. H. Richards, J. R. Winkler, H. B. Gray. *Science* **268**, 1733–1735 (1995).

24   M. J. Bjerrum, D. R. Casimiro, I.-J. Chang, A. J. Di Bilio, H. B. Gray, M. G. Hill, R. Langen, G. A. Mines, L. K. Skov, J. R. Winkler, D. S. Wuttke. *J. Bioenerg. Biomemb.* **27**, 295–302 (1995).

25   K. Sigfridsson, M. Ejdeback, M. Sundahl, O. Hansson. *Arch. Biochem. Biophys.* **351**, 197–206 (1998).

26   K. Sigfridsson, M. Sundahl, M. J. Bjerrum, O. Hansson. *JBIC* **1**, 405–414 (1996).

27   A. J. Di Bilio, C. Dennison, H. B. Gray, B. E. Ramirez, A. G. Sykes, J. R. Winkler. *J. Am. Chem. Soc.* **120**, 7551–7556 (1998).

28   J. R. Winkler, B. G. Malmström, H. B. Gray. *Biophys. Chem.* **54**, 199–209 (1995).

29   C. C. Moser, J. M. Keske, K. Warncke, R. S. Farid, P. L. Dutton. *Nature* **355**, 796–802 (1992).

30   J. R. Winkler, H. B. Gray. *Chem. Rev.* **92**, 369–379 (1992).

31   G. McLendon, R. Hake. *Chem. Rev.* **92**, 481–490 (1992).

32   D. W. Conrad, H. Zhang, D. E. Stewart, R. A. Scott. *J. Am. Chem. Soc.* **114**, 9909–9915 (1992).

33   J. R. Scott, A. Willie, M. Mark, P. S. Stayton, S. G. Sligar, B. Durham, F. Millett. *J. Am. Chem. Soc.* **115**, 6820–6824 (1993).

34   M. B. Twitchett, J. C. Ferrer, P. Siddarth, A. G. Mauk. *J. Am. Chem. Soc.* **119**, 435–436 (1997).

35   B. S. Brunschwig, S. Ehrenson, N. Sutin. *J. Phys. Chem.* **90**, 3657–3668 (1986).

36 B. S. Brunschwig, S. Ehrenson, N. Sutin. *J. Phys. Chem*. **91**, 4714–4723 (1987).

37 B. S. Brunschwig, N. Sutin. *Comments Inorg. Chem*. **6**, 209–235 (1987).

38 T. M. McCleskey, J. R. Winkler, H. B. Gray. *J. Am. Chem. Soc*. **114**, 6935–6937 (1992).

39 T. J. Meade, H. B. Gray, J. R. Winkler. *J. Am. Chem. Soc*. **111**, 4353–4356 (1989).

40 G. M. Brown, N. Sutin. *J. Am. Chem. Soc*. **101**, 883–892 (1979).

41 M. D. Newton. *J. Phys. Chem*. **92**, 3049–3056 (1988).

42 J. J. Hopfield. *Proc. Natl. Acad. Sci. USA* **71**, 3640–3644 (1974).

43 H. M. McConnell. *J. Chem. Phys*. **35**, 508–515 (1961).

44 J. W. Verhoeven. *Adv. Chem. Phys*. **106**, 603–644 (1999).

45 M. N. Paddon-Row. *Acc. Chem. Res*. **27**, 18–25 (1994).

46 M. R. Wasielewski. In *Distance Dependencies of Electron-Transfer Reactions* (M. A. Fox, M. Chanon, eds), Elsevier, Amsterdam (1988).

47 C. Liang, M. D. Newton. *J. Phys. Chem*. **96**, 2855–2866 (1992).

48 C. Liang, M. D. Newton. *J. Phys. Chem*. **97**, 3199–3211 (1993).

49 L. A. Curtiss, C. A. Naleway, J. R. Miller. *Chem. Phys*. **176**, 387–405 (1993).

50 M. J. Shephard, M. N. Paddon-Row, K. D. Jordan. *Chem. Phys*. **176**, 289–304 (1993).

51 D. N. Beratan, J. N. Onuchic, J. J. Hopfield. *J. Chem. Phys*. **86**, 4488–4498 (1987).

52 J. N. Onuchic, D. N. Beratan. *J. Chem. Phys*. **92**, 722–733 (1990).

53 J. N. Onuchic, D. N. Beratan, J. R. Winkler, H. B. Gray. *Annu. Rev. Biophys. Biomol. Struct*. **21**, 349–377 (1992).

54 D. N. Beratan, J. N. Betts, J. N. Onuchic. *J. Phys. Chem*. **96**, 2852–2855 (1992).

55 D. N. Beratan, J. N. Betts, J. N. Onuchic. *Science* **252**, 1285–1288 (1991).

56 J. J. Regan, A. J. Di Bilio, R. Langen, L. K. Skov, J. R. Winkler, H. B. Gray, J. N. Onuchic. *Chem. Biol*. **2**, 489–496 (1995).

57 J. J. Regan, B. E. Ramirez, J. R. Winkler, H. B. Gray, B. G. Malmström. *J. Bioenerg. Biomemb*. **30**, 35–39 (1998).

58 O. Farver, I. Pecht. *JBIC* **2**, 387–392 (1997).

59 J. R. Winkler, H. B. Gray. *JBIC* **2**, 399–404 (1997).

60 C. C. Moser, C. C. Page, X. Chen, P. L. Dutton. *JBIC* **2**, 393–398 (1997).

61 R. J. P. Williams. *JBIC* **2**, 373–377 (1997).

62 A. J. Di Bilio, M. G. Hill, N. Bonander, B. G. Karlsson, R. M. Villahermosa, B. G. Malmström, J. R. Winkler, H. B. Gray. *J. Am. Chem. Soc*. **119**, 9921–9922 (1997).

63 L. K. Skov, T. Pascher, J. R. Winkler, H. B. Gray. *J. Am. Chem. Soc*. **120**, 1102–1103 (1998).

64 R. Langen. PhD Thesis, California Institute of Technology (1995).

65 M. D. Lowery, E. I. Solomon. *Inorg. Chim. Acta* **200**, 233–243 (1992).

66 J. A. Guckert, M. D. Lowery, E. I. Solomon. *J. Am. Chem. Soc*. **117**, 2817–2844 (1995).

67 J. N. Gehlen, I. Daizadeh, A. A. Stuchebrukhov, R. A. Marcus. *Inorg. Chim. Acta* **243**, 271–282 (1996).

68 I. Daizadeh, J. N. Gehlen, A. A. Stuchebrukhov. *J. Chem. Phys*. **106**, 5658–5666 (1997).

69 C. Turro, C. K. Chang, G. E. Leroi, R. I. Cukier, D. G. Nocera. *J. Am. Chem. Soc*. **114**, 4013–4015 (1992).

70 P. J. F. de Rege, S. A. Williams, M. J. Therien. *Science* **269**, 1409–1413 (1995).

71 O. Farver, L. K. Skov, M. Vandekamp, G. W. Canters, I. Pecht. *Eur. J. Biochem*. **210**, 399–403 (1992).

72 O. Farver, I. Pecht. *Biophys. Chem*. **50**, 203–216 (1994).

73 R. Langen, J. L. Colón, D. R. Casimiro, T. B. Karpishin, J. R. Winkler, H. B. Gray. *JBIC* **1**, 221–225 (1996).

74 D. R. Casimiro. PhD Thesis, California Institute of Technology (1994).

75 N. A. Farrow. PhD Thesis, California Institute of Technology (1999).

76 I. V. Kurnikov. PhD Thesis, University of Pittsburgh (1999).

77 W. B. Connick, A. J. Di Bilio, W. P. Schaefer, H. B. Gray. *Acta Cryst. C* **55**, 913–916 (1999).

78 W. B. Connick, A. J. DiBilio, M. G. Hill, J. R. Winkler, H. B. Gray. *Inorg. Chim. Acta* **240**, 169–173 (1995).